Conference paper

Riccardo Checchetto*, Daniele Rigotti, Alessandro Pegoretti and Antonio Miotello

Chloroform desorption from poly(lactic acid) nanocomposites: a thermal desorption spectroscopy study

https://doi.org/10.1515/pac-2018-1216

Abstract: Biopolymer nanocomposites were prepared by solvent casting dispersing lauryl-functionalized cellulose nano-fibrils (CNF) in a poly(lactic acid) matrix (PLA). The release of residual chloroform ($CHCl_3$) solvent molecules was studied by Thermal Desorption Spectroscopy (TDS) analysis. TDS spectra of the PLA matrix show a single desorption peak at $T_P = 393$ K with FWHM ~10 K, compatible with a zero-order desorption kinetics. This narrow TDS peak was accurately reproduced assuming that: (i) the rate limiting step is given by the $CHCl_3$ de-trapping from sites in the PLA matrix where residual solvent molecules form small aggregates and (ii) the activation energy for desorption linearly decreases from 1.19 eV for saturated traps to 1.11 eV when the traps occupancy by solvent molecules approaches zero. The balance energy term $\varepsilon_D = -0.08$ eV is due to the attractive interactions between trapped $CHCl_3$ molecules. Adding CNF particles to the PLA matrix the zero-order peak shifts to lower temperatures and a second peak with FWHM ~60 K appears at higher temperatures. This second peak is compatible with a first-order desorption kinetics and is attributed to the release of dispersed $CHCl_3$ molecules from trapping sites in PLA-CNF interface region. The obtained information are of interest for applications in food and electronic packaging and for the development of medical materials.

Keywords: biopolymer nanocomposites; Eurasia 2018; nano-cellulose; poly(lactic acid); solvent release; Thermal Desorption Spectroscopy.

Polylactic acid (PLA) is a biopolymer with high optical transparency and good workability properties which is currently investigated for the replacement of commercial petroleum-based polymers in packaging technology [1]. The addition of bio-based nanoparticles such as nano-cellulose [2] has demonstrated a reliable way to improve the PLA mechanical properties, thermal stability [3]. Moreover cellulose nanofibers have been investigated as additive particle in biopolymer films due to their ability to improve the barrier properties against water [4], water vapor [5], air and oxygen [6] and CO_2 [7]. Cellulose nanofibrils (CNF) are elongated nanoparticles extracted from cellulose by acid hydrolysis having diameter ~ few nm and length in the 100 nm range with both amorphous and crystalline regions: CNF are of great interest given their gas-impermeable nature, high optical transparency and excellent mechanical properties [2]. A reliable process for the production of PLA-CNF nanocomposite films is the solvent casting method [8, 9]. This process involves the dissolution of polymer pellets in a solvent which is then loaded with the proper amount of filler nanoparticles,

Article note: A collection of invited papers based on presentations at the 15th Eurasia Conference on Chemical Sciences (EuAsC2S-15) held at Sapienza University of Rome, Italy, 5–8 September 2018.

***Corresponding author: Riccardo Checchetto,** Department of Physics, University of Trento, Via Sommarive 14, I-38123, Trento, Italy, e-mail: riccardo.checchetto@unitn.it
Daniele Rigotti and Alessandro Pegoretti: Department of Industrial Engineering, University of Trento, Via Mesiano 77, I-38123, Trento, Italy
Antonio Miotello: Department of Physics, University of Trento, Via Sommarive 14, I-38123, Trento, Italy

previously surface functionalized to favor their dispersion in the nanocomposites. The resulting solution is then poured onto a glass plate where it is then dried to form a film. Residual solvent tend to remain in the casted film after drying [10].

In this communication we present an experimental study on the desorption kinetics of residual solvent molecules (chloroform, $CHCl_3$) from biopolymer nanocomposites consisting of lauryl-functionalized cellulose nano-fibrils (CNF) particles dispersed in a poly(lactic acid). The solvent desorption kinetics was studied in structurally characterized nanocomposites by Thermal Desorption spectroscopy (TDS) using a Quadrupole Mass Spectrometer (QMS). The obtained TDS spectra were then analyzed fitting experimental data by curves obtained through a model describing the transport of the $CHCl_3$ molecules hosted in the PLA matrix to the sample surface where their desorption occurs. We obtained information on the physical-chemical state of the residual solvent molecules in the PLA layers and a description of the microscopic mechanism controlling their release. Information on the residual solvent desorption kinetics are important for applications in particular in fields such as food and electronic packaging, as well as for the development of innovative medical material [11–13]. The obtained information are also of basic interest because the role of residual solvent in the dispersion of the filler particles in the casted polymer films, which determines different properties of the nanocomposite, is not well investigated [14–17].

PLA nanocomposites were prepared by solution mixing and casting according to the following procedure. A first solution was prepared dissolving poly(lactic acid) (PLA 4032D, Nature works LLC, density of 1.24 g/cm^3 and 160 °C melting point) in $CHCl_3$ (1 g PLA/25 ml $CHCl_3$) under magnetic stirring at 40 °C. Cellulose nano-fibrils were obtained from cotton through acid hydrolysis and were functionalized by grafting hydrophobic lauryl chain via esterification. A second solution was then prepared by dissolving the laury-functionalized cellulose nano-fibrils [7] in $CHCl_3$ (0.1 g CNF/10 ml $CHCl_3$) using ultra-sonicator at 200 W in an ice bath. The PLA-$CHCl_3$ and CNF–$CHCl_3$ solutions were then mixed together by magnetic stirrer for 3 h. Nanocomposite films having different additive content were obtained casting mixed solutions with proper PLA-CNF weight ratio in a petri dish after solvent evaporation at room temperature for 24 h and then in a ventilated oven at 40 °C for 4 h. Pure PLA films 49 ± 1 μm thick and nanocomposite films with 3 wt. % and 5 wt. % LNC content having thickness of 53 ± 1 and 52 ± 1 μm, respectively, have been examined.

Information on the nanocomposite structure and on the dispersion degree of the filler particles were obtained by Scanning Electron Microscopy (SEM) analyzing the LN_2 fractured cross-sections of nanocomposite films (JEOL high resolution Field Emission Scanning Electron Microscope at 5 kV accelerating voltage). The SEM micrograph in Fig. 1a shows the cross-section of the pure PLA film which presents a smooth and uniform morphology without specific structures. Micrographs in Fig. 1b,c show the cross-section of the nanocomposite sample with 3 and 5 wt. % additive content, respectively: here cavities with not uniform size and shape are present and dispersed filler particles can be distinguished in the cavity walls (see dashed circles). Occasionally, in the nanocomposite with 5 wt. % filler content, CNF aggregates with sub-micrometer size and irregular shape can be observed. SEM micrographs, presented in a previous paper, show that at filler content larger than ~6 wt. % a relevant fraction of the CNF filler particles form CNF aggregates with size in the few micrometer range [7].

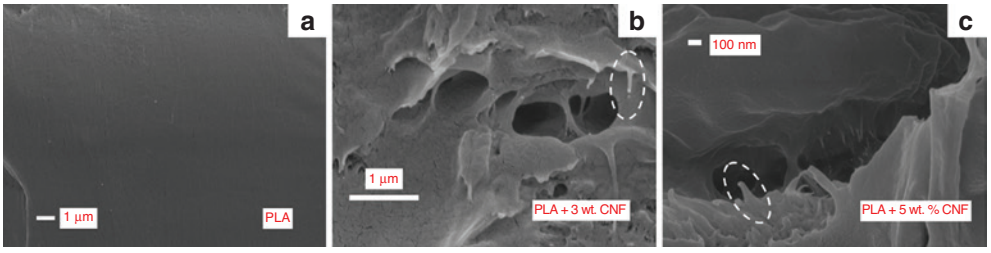

Fig. 1: Cross-sectional SEM micrographs of the pure PLA sample (a), PLA + 3 wt. % CNF (b) and PLA + 5 wt. % CNF (c) nanocomposites.

Figure 2a shows the DSC spectra of the pure and nanocomposite samples (Mettler Toledo TC15 calorimeter, 10 mg samples, N_2 flow of 150 ml/min at 10 °C/min). The addition of CNF filler particles does not influence the glass transition temperature value $T_g = 330$ K, nor the melting temperature value $T_m = 438$ K. The most relevant change shown by the DSC spectra is the decrease of the PLA crystalline fraction from 2.7 % for the pure PLA to 1.4 % for the PLA nanocomposite with 5 wt. % CNF [7]. We also note that the crystallization peak at ~400 K shown by the pure PLA disappears introducing the CNF additive. Figure 2b shows the thermogravimetric curves obtained in the 300–700 K temperature interval at a heating rate of 10 K/min, under a nitrogen flow of 150 ml/min (TGA Q5000 from TA instrument). The TGA curve of the pure PLA sample shows same features as the nanocomposites: (i) a first mass loss starting at ~350 K and (ii) a single step decomposition process starting at ~600 K with maximum decomposition rate at ~640 K.

The kinetics of the residual $CHCl_3$ solvent desorption process was studied by Thermal Desorption Spectroscopy (TDS) using film samples with 2×5 mm size and thickness values reported above. Experiments were carried out monitoring the $CHCl_3$ mass signal during sample heating in a continuously pumped UHV chamber from $T_0 = 300$ K to $T_f = 500$ K, which is below the sample decomposition temperature, with a linear temperature ramp of pendency $\alpha = 0.12$ K/s. The solvent desorption signal was monitored by a Quadrupole Mass Spectrometer (QMS) equipped with grid-type ion source (operating at 90 V ionization potential) and Secondary Electron Multiplier acquiring the QMS $I_{m/e}$ ion currents pertinent to the $CHCl_3$ fragmentation products: $m/e = 83$, 85 and 47 [18]. The $I_{m/e}$ QMS signal is proportional to the $CHCl_3$ partial pressure P_{CHCl_3} : under continuous pumping conditions P_{CHCl_3} is a measure of the $CHCl_3$ desorption rate $j_{des}(t) = \frac{S_p}{A} P_{CHCl_3}$ where S_p is the pumping speed of the vacuum system and A the "effective" surface area of the film sample [19]. Relative indeterminations in the $CHCl_3$ desorption signal are evaluated by the relation $\delta I_{m/e}^{back} / I_{m/e}$ where $\delta I_{m/e}^{back}$ is the mean value of the fluctuations of the $I_{m/e}^{back}$ background signal [20]. Before gas transport tests, the nanocomposite sample was kept in UHV conditions at 300 K inside the experimental apparatus for at least 10 h.

The normalized TDS spectrum of the pure PLA sample is shown in Fig. 3: experimental data are presented as open symbols while the experimental indeterminations are inside the size of the symbol. Solid lines are fitting of the experimental data, see text below. The spectrum exhibits a single, narrow desorption peak centered at temperature $T_P = 393 \pm 1$ K with FWHM ~10 K: this peak presents an exponentially increasing leading edge at $T \cong 340$ K and a sudden high-temperature cut-off at $T \cong 400$ K which are features typical of zero-order desorption kinetics [21]. Note that the desorption process occurs in the same temperature range where TGA analysis evidences the first mass loss, see right panel of Fig. 2; note also that solvent release occurs in the $T_g < T < T_m$ temperature interval, see left panel of Fig. 2.

The normalized TDS spectra pertinent to the PLA nanocomposites with 3 and 5 wt. % filler content are presented in Figs. 4 and 5, respectively. These spectra appear more structured than that of the pure sample. The spectrum of the PLA + 3 wt. % CNF nanocomposite presents, in fact, a shoulder in the high temperature

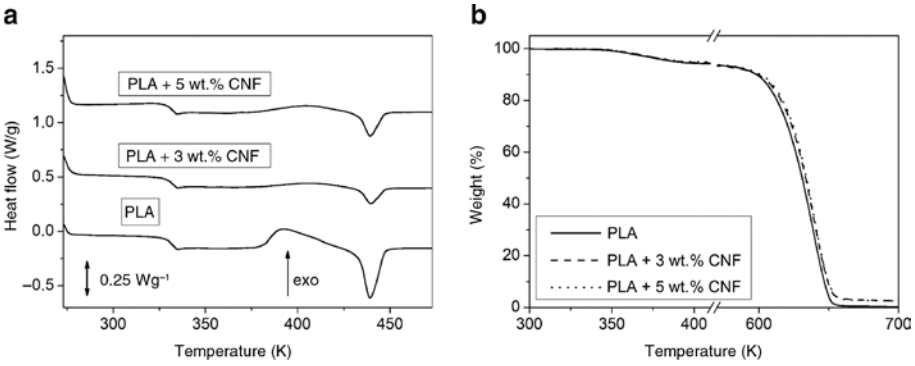

Fig. 2: DSC spectra of pure PLA and of the PLA nanocomposites with 3 and 5 wt. % CNF content (a). Thermo-gravimetric curves of pure PLA and of the PLA nanocomposites with 3 and 5 wt. % CNF content (b).

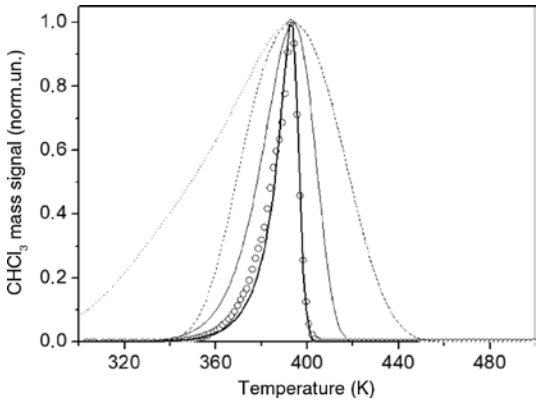

Fig. 3: Open symbols: $CHCl_3$ TDS spectrum of PLA. Lines: TDS curves numerically obtained assuming different solvent transport processes. Dashed and dotted lines: diffusion- controlled transport mechanism with $E_{diff} = 0.5$ eV and $D_0 = 8 \times 10^{-3}$ cm^2/s (see text). Thin solid line: de-trapping model with $E_{des} = 1.17$ eV, $p_0 = 1.0 \times 10^{13}$ s^{-1} and $\varepsilon_D = 0$. Thick solid line: de-trapping model with $E_{des} = 1.11$ eV, $p_0 = 1.0 \times 10^{13}$ s^{-1} and $\varepsilon_D = -0.07$ eV.

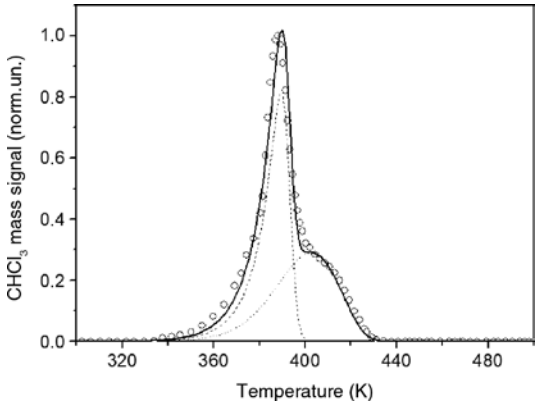

Fig. 4: Open symbols: $CHCl_3$ TDS spectrum of the PLA + 3 CNF wt. % nanocomposite. Dashed line: de-trapping model with $E_{des} = 1.11$ eV, $p_0 = 1.0 \times 10^{13}$ s^{-1} and $\varepsilon_D = -0.08$ eV. Dotted line: de-trapping model with $E_{des} = 1.21$ eV, $p_0 = 1.0 \times 10^{13}$ s^{-1} and $\varepsilon_D = 0$. Solid line: convolution of dotted and dashed lines.

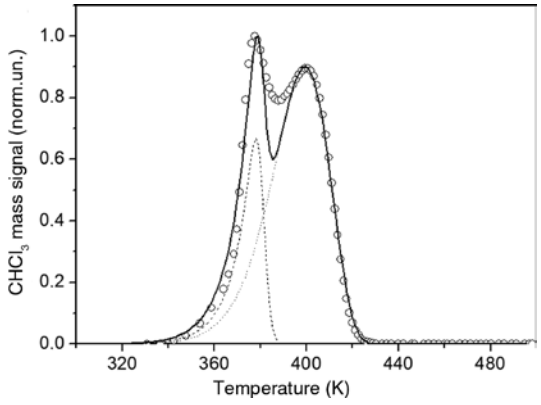

Fig. 5: Open symbols: $CHCl_3$ TDS spectrum of the PLA + 5 CNF wt. % nanocomposite. Dashed line: de-trapping model with $E_{des} = 1.07$ eV, $p_0 = 1.0 \times 10^{13}$ s^{-1} and $\varepsilon_D = -0.07$ eV. Dotted line: de-trapping model with $E_{des} = 1.20$ eV, $p_0 = 1.0 \times 10^{13}$ s^{-1} and $\varepsilon_D = 0$. Solid line: convolution of dotted and dashed lines.

side of the peak at $T_P = 388 \pm 1$ K. The spectrum of the PLA + 5 wt. % CNF nanocomposite consists of two partially overlapping narrow peaks with similar intensity centered at $T_{P,a} = 377 \pm 1$ K and $T_{P,b} = 400 \pm 1$ K.

The desorption of molecules dispersed in a host matrix is composed by three processes: (i) the release (de-trapping) of the particles from matrix sites (traps) where they are preferentially hosted, (ii) their diffusion to the matrix surface and (iii) their desorption from surface sites. According to this model, the concentration of $CHCl_3$ molecules $c(x, t)$ in free volume sites of the host matrix changes with time according to the following continuity equations:

$$\frac{\partial c(x,t)}{\partial t} = D\frac{\partial^2 c(x,t)}{\partial^2 x} + N_0\, p\, \theta(x,t) \tag{1a}$$

$$\frac{\partial \theta(x,t)}{\partial t} = -p\,\theta(x,t) \tag{1b}$$

In eq. 1(a) N_0 is the density of trapping sites per unit volume in the $x = [0, h]$ domain, $x = 0$ and $x = h$ are the film opposite surfaces and x the direction along which net solvent transport occurs. Because $x \ll L$ edge effects can be neglected and the transport problem can be studied in a 1-dimensional geometry. $\theta(x, t)$ is the fractional occupancy at time t of the traps sites located at depth $0 < x < h$: trap saturation occurs when $\theta(x, t) = 1$ while $\theta(x, t) = 0$ indicates empty sites. This model assumes two simplifying hypotheses: (i) freely diffusing $CHCl_3$ molecules released from trap sites cannot by trapped again and (ii) trap sites are isolated and there is no path for the transfer of molecules between traps. The previous equation is numerically solved with the following boundary conditions:

$$c(x = 0, t) = c(x = h, t) = 0 \tag{2}$$

which hold as the sample surface layers are exposed to the vacuum in the pumped UHV chamber; the solvent desorption flux $j(t)$ was then calculated by the relation:

$$j(t) = D\left(\frac{\partial c(x,t)}{\partial x}\right)_{x=0} - D\left(\frac{\partial c(x,t)}{\partial x}\right)_{x=h} \tag{3}$$

The molecular diffusivity D which control the solvent transport to the surface sites and the de-trapping parameter p which controls the molecular release from trap sites, are fitting parameters of this model. During the TDS run, D changes with temperature $T(t) = T_0 + \alpha t$ according to the Arrhenius relation $D(T) = D_0 \exp\left(-\frac{E_{\text{diff}}}{k_B\, T(t)}\right)$ where E_{diff} is the activation energy for $CHCl_3$ diffusion in PLA and D_0 the pre-exponential factor. The $p = p(T)$ parameter describes the probability that a trapped molecules is released from the trap site: it is proportional to the oscillation frequency of the molecule in the trapping site p_0 and the probability that after an oscillation the molecule escapes from the trap which depends on the trapping energy E_{des}. This parameter also changes during the TDS ramp according to the Arrhenius relation $p(T) = p_0 \exp\left(-\frac{E_{\text{des}}(\theta)}{k_B\, T(t)}\right)$.

To describe possible interactions between $CHCl_3$ molecules in trapping sites we introduce a θ-dependent activation energy for desorption:

$$E_{\text{des}}(\theta) = E^0_{\text{des}} - \varepsilon_D \theta \tag{4}$$

where E^0_{des} is the activation energy for desorption of solvent molecules from trapping sites at low fractional occupancy while the ε_D term describes attractive ($\varepsilon_D < 0$) or repulsive ($\varepsilon_D > 0$) interactions between trapped molecules. Note that the ε_D term plays in the present system the role of the "lateral" interaction term in the Elovich equation, thus describing interaction between adsorbed neighboring molecules in surface processes [22, 23].

As a first attempt we assumed that solvent molecules are hosted only in free volume sites of the host matrix, $\theta(x, t=0)$, and modeled the solvent desorption as diffusion-controlled process [24]. We have not found information on the $CHCl_3$ diffusivity in PLA and thus reasonable values of the E_{diff} and D_0 parameters have to be guessed. In the simulations we have assumed a lower limit of 0.35 eV for E_{diff} which correspond to the activation energy of diffusion for CO_2 diffusion in PLA [25] and different $c(x, t=0)$ profiles as initial solvent concentration in the PLA layers. Simulated TDS curves cannot reproduce the experimental TDS spectra. Each (E_{diff}, D_0) parameters couple that produces TDS curves with the correct peak position at $T_P = 393 \pm 1$ K, gives rise to peak having shape different to the observed one: simulated peaks, in fact, present much larger FWHM than experimentally observed. The dashed line in Fig. 3, for example, was obtained with narrow Gaussian $c(x, t=0)$ profile with $x_0 = 25$ μm and $\sigma = 1$ μm: this curve presents a TDS peak with FHWM ~50 K. Even larger FWHM are observed with TDS curves obtained with uniform $c(x, t=0) = c_0$ profiles, see dotted line in Fig. 3.

We then modeled the solvent desorption assuming that the transport of solvent molecules to the sample surface is a fast process: the release of solvent molecules from their trapping sites controls the desorption of solvent $CHCl_3$ molecules from the nanocomposite samples. The $CHCl_3$ desorption flux j_{des} is thus proportional to the solvent release rate r:

$$r = -\frac{\partial \theta(x,t)}{\partial t} = p\,\theta(x,t) = p\,\theta(t) \tag{5}$$

As an attempt we assumed $\varepsilon_D = 0$ and we solved Eq. 5 with the initial condition $\theta(t=0) = \theta_0 = 1$. To avoid an arbitrary choice of the pre-exponential factor we fixed it at $p_0 = \frac{k_B T}{h} \sim 1.0 \times 10^{13}$ s^{-1} which is a common chosen value in TDS data analysis [26].

The experimental TDS peak position was reproduced with $E_{des} = 1.17$ eV, see thin solid line in Fig. 3: here also, similarly to that observed with the diffusion model, the obtained spectrum fails in reproducing the shape and FWHM of the observed one. The TDS peak presents, in fact, a symmetrical shape and much broader FWHM than experimentally observed.

The experimental TDS spectrum of the pure PLA sample was accurately reproduced considering the presence of lateral interactions between the trapped molecules: the thick solid line in Fig. 3 fitting the experimental TDS spectrum was, in fact, obtained with $E^0_{des} = 1.11\,eV$, $p_0 = 1.0 \times 10^{13}$s^{-1} and $\varepsilon_D = -0.08$ eV. Note that the obtained TDS curves exhibits the typical shape of zero-order desorption processes with the same FWHM as the observed TDS spectrum.

Figure 6 shows, as a function of temperature T, quantities relevant to describe the present desorption process, namely the fractional occupancy term θ and the simulated desorption curve in the upper panel, the p parameter in lower panel when $E_{des}(\theta) = E^0_{des} - \varepsilon_D\,\theta$ and, for sake of comparison, when $E_{des}(\theta) = E^0_{des}$. This figure describes the correlation between these quantities and illustrates the apparent zero-order kinetics of the desorption process. Specifically, comparing the θ and p curves, we observe that the $\varepsilon_D\theta$ term in $E_{des}(\theta)$ forces the desorption constant p keeping low value of as long as $\theta \sim 1$. When trapping sites start to release trapped molecules, that is θ diminishes, then the $\varepsilon_D\theta$ term reduces and a fast increase of the de-trapping constant p occurs: this fast increase triggers a self- sustaining "explosive" desorption process having as fingerprint the very narrow TDS peak and the apparent zero-order kinetics.

Before going on with the discussion it is worthy to mention that extrended simulation works considering the complete diffusion-detrapping model, as described by eqs. 1(a,b), has revealed that the shape and position of the simulated TDS curves do not change changing diffusion-related parameters such as sample size h or the initial distribution profiles $\theta(x, t=0)$ of the trapped molecules, as long as the activation energy for diffusion E_{diff} is lower than E_{des}. The fast diffusion process of solvent molecules is clearly connected to the fact that: (i) the PLA matrix is in its rubbery phase and (ii) kinetic processes occur at temperatures $T \sim T_m$ (see DSC in Fig. 2).

Thermal desorption processes of molecules adsorbed at the solid surfaces exhibit apparent zero-order kinetics when a fraction of adsorbed molecules form aggregates acting, as long as they are present, as a

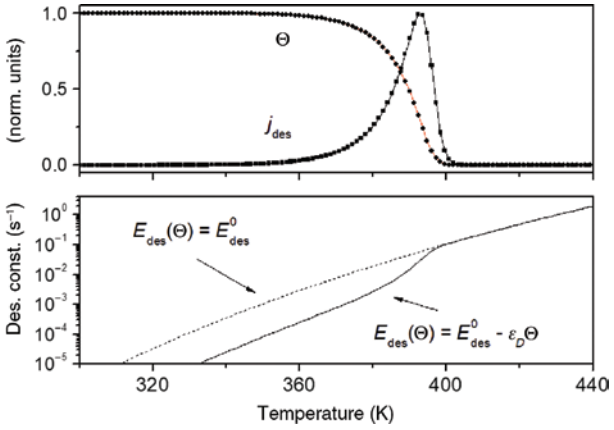

Fig. 6: Upper panel: TDS curve (j_{des}) and fractional occupancy θ as a function of temperature (simulated curves). Lower panel: desorption constant p obtained with $E_{des}(\theta) = E^0_{des} - \varepsilon_D\theta$ (solid line) and with $E_{des}(\theta) = E^0_{des}$ (dashed line) as a function of temperature. Curves were obtained with $E^0_{des} = 1.11$ eV, $p_0 = 1.0 \times 10^{13}$ s^{-1} and $\varepsilon_D = -0.08$ eV.

reservoir to maintain constant the surface coverage: the "lateral" energy term is negative describing attractive interactions between aggregated molecules [21, 26, 27].

The obtained ε_D value of −0.08 eV indicates that residual solvent molecules attractively interact forming aggregates in open volumes (cavities) reasonably located in the boundary layers between the amorphous and crystalline regions of the present semi-crystalline polymer [28, 29]. Molecules hosted in filled trapping sites ($\theta \sim 1$), due to their attractive interaction, have to overcome a potential energy barrier which is $\varepsilon_D \sim 0.08$ eV larger than that in empty trapping sites ($\theta \sim 0$).

It is worthy to mention that the obtained ε_D value well compare with values found in different surface studies. Nagai, for example, analyzing TDS spectra of the Xe/CO/W(110) system evaluated an interaction energy term of 0.88 kcal/mol ≅ 0.04 eV [30]. Varma and Dowben analyzing N_2 desorption spectra from Ni surfaces obtained a value of 5 kJ/mol ≅ 0.05 eV which increased when N_2 molecules formed ordered over-layers [31]. Hood *et al.* finally, obtained a values of 0.45 kcal/mol ≅ 0.02 eV in N_2 desorption processes from Ru(001) surfaces [32]. Note also that the present values are of the same order as the minimum of the Lennard-Jones potential energy curve between like molecules, Xe–Xe: 0.0197 eV, CO_2–CO_2: 0.0163 eV, CH_4–CH_4: 0.0118 eV [33] and suggests that the trapped molecule interacts with the next-neighbor ones [30–32].

Let us consider now the TDS spectra of the PLA nanocomposites in Figs. 4 and 5. These spectra can be reproduced by the overlapping two TDS peaks both obtained assuming the $CHCl_3$ de-trapping process as rate limiting step in the desorption kinetics. The first peak, see dashed lines in Figs. 4 and 5, shows FWHM ~ 10 K, is compatible with a zero-order desorption kinetics and is due to solvent de-trapping from aggregates in the PLA matrix. In fact, it can be accurately reproduced with $p_0 = 1.0 \times 10^{13}$ s^{-1}, $\varepsilon_D = -0.07$ eV and activation energies similar to those of the pure PLA film: $E^0_{des} = 1.1$ eV in the nanocomposite with 3 wt. % filler content and 1.07 eV in the nanocomposite with 5 wt. filler content. The second peak, see dotted lines in Figs. 4 and 5, shows a larger FWHM, ~60 K, and its shape is compatible with a first-order desorption kinetics. This peak was reproduced with $p_0 = 1.0 \times 10^{13}$ s^{-1} but: (i) larger activation energy for desorption $E^0_{des} = 1.21$ eV in the nanocomposite with 3 wt. % filler content and $E^0_{des} = 1.20$ eV in the nanocomposite with 5 wt. % filler content and (ii) $\varepsilon_D = 0$. SEM analysis indicate that in both samples CNF particles are well dispersed in the PLA matrix layers, see Fig. 1, without changing its crystalline fraction and T_g value as indicated by the DSC tests. Given the impermeable nature of nano-cellulose, the second TDS peak can be tentatively attributed to the release of dispersed $CHCl_3$ molecules trapped in interface sites between PLA matrix and surface-functionalized additive. The comparison between the integrated areas of the two TDS peaks indicates that this second contribution increases with the filler content as it accounts for the release of ~46 % and ~75 % solvent molecules in the nanocomposite with 3 and 5 wt. % filler content, respectively.

In conclusion, PLA-based biopolymer nanocomposites were prepared by solvent casting method with filler contents up to 5 wt. %. TDS spectra reveal that the release of residual $CHCl_3$ solvent molecules occurs when the PLA matrix is in its rubbery phase from two kind of trapping sites. The solvent release from the PLA matrix follows an apparent zero-order desorption kinetics and the obtained TDS spectra can be reproduced assuming that solvent release is controlled by the thermally activated de-trapping of aggregated $CHCl_3$ molecules attractively interacting. The addition of filler particles introduces supplementary trapping sites where dispersed $CHCl_3$ molecules are hosted.

Acknowledgements: The support of N. Bazzanella (Dept. of Physics, University of Trento) in SEM analysis is gratefully acknowledged. Prof. D. Caretti and dr. M. Rizzuto (University of Bologna, Italy) are kindly acknowledged for the provision of the lauryl functionalized nanocellulose.

References

[1] M. Jamshidian, E. A. Tehrany, M. Imran, M. Jacquot, S. Desobry. *Compr. Rev. Food Sci. Food Saf.* **9**, 552 (2010).
[2] A. Dufresne. *Mat. Today* **16**, 220 (2013).
[3] W. D. Ding, M. Pervaiz, M. Sain. in *Functional Biopolymers*, V. Thakur, M. Thakur (Eds.), pp. 183–216, Springer Series on Polymer and Composite Materials, Springer, Cham (2018).
[4] M. D. Sanchez-Garcia, E. Gimenez, J. M. Lagaron. *Carbohydr. Polym.* **71**, 235 (2008).
[5] A. Khan, R. A. Khan, S. Salmieri, C. Le Tien, B. Ridl, J. Bouchard, G. Chauve, V. Tan, M. R. Kamal, M. Lacroix. *Carbohydr. Polym.* **90**, 1601 (2012).
[6] N. Lavoine, I. desloges, A. Dufresne, J. Bras. *Carbohydr. Polym.* **90**, 735 (2012).
[7] D. Rigotti, R. Checchetto, S. Tarter, D. Caretti, M. Rizzuto, L. Fambri, A. Pegoretti. *Expr. Polym. Lett.* **13**, 858 (2019).
[8] M. Jonoobi, A. P. Mathew, M. M. Abdi, M. D. Makinejad, K. J. Oksman. *Polym. Environ.* **20**, 991 (2012).
[9] J. Trifol, D. Plackett, C. Sillard, P. Szabo, J. Bras, A. E. Daugaard. *Polym. Int.* **65**, 988 (2016).
[10] U. Siemann. in *Scattering Methods and the Properties of Polymer Materials. Progress in Colloid and Polymer Science*, N. Stribeck, B. Smarsly (Eds.), vol. 130, Springer, Berlin (2005).
[11] Y. H. Hwang, T. Matsui, T. Hanada, M. Shimoda, K. Matsumoto, Y. Osajima. *J. Agric. Food Chem.* **48**, 4310 (2000).
[12] B. Muir, H. B. Duffy, M. C. Moran. *J. Chromatogr. A* **1038**, 183 (2004).
[13] S. C. Anand, J. F. Kennedy, M. Miraftab, S. Rajendran. *Medical Textiles and Biomaterials for Healthcare*. CRC Press, Boca Raton (2006).
[14] N. Jouault, D. Zhao, S. K. Kumar. *Macromolecules* **47**, 5246 (2014).
[15] D. W. Janes, J. F. Moll, S. E. Harton, C. J. Durning. *Macromolecules* **44**, 4920 (2011).
[16] S. J. Meth, S. G. Zane, C. Z. Chi, J. D. Londono, B. A. Wood, P. Cotts, M. Keating, W. Guise, S. Weigand. *Macromolecules* **44**, 8301 (2011).
[17] H. Lin, A. Dufresne. *Eur. Polym. J.* **59**, 302 (2014).
[18] J. P. Johnson, L. G. Christophorou, J. G. Carter. *J. Chem. Phys.* **67**, 2196 (1977).
[19] P. A. Redhead, J. P. Hobson, E. V. Kornelsen. *The Physical Basis of Ultrahigh Vacuum*, pp. 423, American Institute of Physics, New York (1993).
[20] R. Checchetto, P. Bettotti, R. S. Brusa, G. Carotenuto, W. Egger, C. Hugenschmidt, A. Miotello. *Phys. Chem. Chem. Phys.* **20**, 24617 (2018).
[21] V. P. Zhdanov. *Elementary Physicochemical Processes at Solid Surfaces*, pp. 145–189, Springer Science, New York (1991).
[22] A. M. Peers. *J. Catal.* **4**, 499 (1965).
[23] J. W. Niemantverdriet, K. Markert, K. Wandelt. *Appl. Surf. Sci.* **31**, 211 (1988).
[24] W. Bayer, H. Wagner. *J. Appl. Phys.* **53**, 8745 (1982).
[25] L. Bao, J. R. Dorgan, D. Knauss, S. Hait, N. S. Oliveira, I. M. Marrucho. *J. Membrane Sci.* **285**, 166 (2006).
[26] R. I. Masel. *Principles of Adsorption and Reaction on Solid Surfaces*, pp. 482, Wiley, New York (1996).
[27] K. Christmann. *Surface Physical Chemistry*, pp. 152, Steinkoppf, Darmstadt (1991).
[28] M. H. Kloppfer, B. Flaconneche. *Oil Gas Sci. Technol.* **56**, 223 (2001).
[29] W. R. Vieth, K. J. Sladek. *J. Colloid Sci.* **20**, 1014 (1965).
[30] K. Nagai. *Phys. Rev. Lett.* **59**, 2159 (1985).
[31] S. Varma, P. A. Dowben. *J. Vac. Sci. Technol. A* **8**, 2605 (1990).
[32] E. S. Hood, B. H. Toby, W. H. Weinberg. *Phys. Rev. Lett.* **55**, 2437 (1985).
[33] P. A. Redhead, J. P. Hobson, E. V. Kornelsen. *The Physical Basis of Ultrahigh Vacuum*, pp. 15, American Institute of Physics, New York (1993).